DE-FG05-80ET-53088-645 IFSR #645

Magnetically Constricted Intergalactic Plasmas

T. TAJIMA

Department of Physics and Institute for Fusion Studies
The University of Texas at Austin
Austin, Texas 78712

June 1994

Magnetically Constricted Intergalactic Plasmas

T. TAJIMA
Department of Physics and Institute for Fusion Studies
The University of Texas at Austin
Austin, Texas 78712

Abstract

A model of magnetically constricted hot intergalactic plasmas as a source of the cosmic X-ray background radiation satisfies the known observational constraints. The network magnetic fields that weave through clusters of galaxies are strongly constricted by the violent relaxation of the clusters in the supercluster potential. These intercluster fields tend to constrict the trapped plasma, driving them to high densities and high temperatures. These hot ($T \geq 10^8\,\mathrm{K}$) and dense plasmas are magnetically insulated from colder ($T \leq 10^4\,\mathrm{K}$) surrounding gases, forming intermittent intercluster medium. The dynamical processes of these fields involve rapid magnetic relaxation toward the nearly force-free state by involving reconnection of field lines and rapid heating of plasmas by being continuously fed energy from the violent gravitational relaxation. The fundamental physical processes of magnetic constriction and subsequent plasma heating by the violent motions of compact objects that trap the magnetic fields are elucidated. Brightening regions of such magnetically constricted plasmas have typical dimensions of order the size of clusters or even less, thus they will be seen as a diffuse X-ray source. This model explains the large amount of necessary thermal energy that results in cosmic X-ray background radiation in a large supercluster spatial scale, the rapid heating, the

small amount of deviation of the cosmic microwave background radiation due to the Comptonization, and how to keep colder gases from evaporating. Compatible with this model is the primordial origin of magnetic fields. Earlier we demonstrated that the primordial plasma could sustain a large amount of spontaneously generated magnetic fields and thus isothermal density fluctuations with little temperature signatures. We further consider the evolution of such generated magnetic fields by dynamo in the epoch following this and preceding the above X-ray forming epoch. Using the ABC dynamo model, we obtain the cellular morphology of magnetic fields in the expanding Universe.

I. Introduction

The origin of the cosmic X-ray background radiation still remains a puzzle. This can be fitted by the bremsstrahlung from optically thin plasma with $T_X \sim 40\,\mathrm{keV}$. There are two possible candidates for this; a hot, diffuse intergalactic medium (IGM), or sum of unresolved, discrete sources, such as quasars and Seyfert galaxies. In fact, the recent X-ray satellite ASCA could discriminate against such candidates.

In this paper, we consider diffuse intergalactic media as a possible cause of the X-ray background. Especially we assume the presence of global cosmic magnetic fields and discuss if such intergalactic magnetic fields could remove difficulties that existing non-magnetized IGM models are confronted with. There have been many works so far done in the field of the intergalactic medium, but little attention has been paid to the consequence of the violent activity of the magnetic fields.

Guilbert and Fabian (1986) concluded that the X-ray background can be explained if IGM was heated up to $T_X \sim 400\,\mathrm{keV}$ at $z = 3.6$ due to some unknown mechanism (see also Field and Perrenod 1977; Taylor and Wright 1989). There are, however, stringent constraints for possible nature of IGM: According to the recent COBE data of the cosmic microwave background radiation (CMBR), the allowed value for the Compton y parameter is at most 0.001 (Mather *et al.* 1990). The presence of hot radiation inevitably causes, however, the distortion of CMBR via inverse-Compton scattering (e.g. Sunyaev and Zeldovich 1972; Lahav *et al.* 1990). The lack of the Comptonization has a severe constraint on the non-magnetic IGM model for X-ray background. A hot IGM also requires huge mass in the universe, $\Omega_B > 0.2$, whereas the baryon densities, estimated from the theory of primordial nucleosynthesis, give $\Omega_B \sim 0.1$ or less, in apparent contradiction with the results of the IGM hypothesis.

To sum up, a huge amount of energy needed to heat up IGM and little distortion observed in CMBR seems to be a paradox for the (uniform, non-magnetized) IGM model as an origin of X-ray background radiation. There is a possibility for IGM in a two-phase medium; namely an X-ray emitting, hot tenuous region is surrounded by low temperature, dense region. However, to get huge X-ray emissivity we need a certain value of density for a hot medium, and, to make pressure balance, the density of the cool medium should be even larger, requiring large Ω_B. It is also unclear how to stop evaporation of cold gas. Basic physical processes of flux tube constriction that may underlie the phenomenon are surveyed in Sec. II. We discuss this X-ray mechanism in Secs. III and IV. Cosmological fields existed primordially from the fundamental physical reasons (Tajima *et al.* 1991). After such magnetic fields are spontaneously created, they need to grow in spatial size and also to fight against the dilution due to cosmic expansion. This may be realized by the dynamo action. We consider such a possibility by adopting a simple model called the ABC (Arnold-Beltrami-Childress) dynamo model in Secs. V and VI. We note that observational evidence is increasing for large-scale magnetic fields, such as intercluster magnetic fields (Kim *et al.* 1991; Tribble 1991).

II. Basic Physical Processes of Flux Tube Constriction

Before we enter the wave realistic model of a network of magnetic fields anchored in violently moving clusters, we isolate two specific physical processes of flux tube dynamics in this section. The clusters may be moving violently relative to each other, both in terms of the mutual distance and in terms of the mutual orientation. The former will stretch or shorten the tubes, while the latter will twist and kink the tubes. In general, the web of networked magnetic fields undergo the combination of these motions (and wave complicated ones). During such actions the complex geometry of networked fields is often forced to undergo reconnection. This involves the resistive process, accompanied by heating and acceleration

of the plasma trapped in the magnetic field. As a result the topology of magnetic fields changes. In the present section we pick up the twisting motion of the flux tube and its resultant kink instability as a first example and examine the interaction of two flux tubes and their reconnection as a second.

A. Twist and kink of flux tubes

When a flux tube is mechanically twisted at two ends that rotate in the opposite senses, the field lines in the tube get wound up and as a result the field-aligned current ($\mathbf{j} \times \mathbf{B} \approx 0$) is induced. As long as $\mathbf{j} \times \mathbf{B} \approx 0$ (or $\mathbf{j} \times \mathbf{B} = \nabla p$), the plasma stays in equilibrium. However, if the current buildup is above a certain threshold, the entire flux tube now becomes unstable and exhibits a kink instability. In Fig. 1 we show an example (Zaidman and Tajima, 1989) of such a twisted flux tube undergoing the kink instability. Also in this simulation the twisting azimuthal velocity is sheared, i.e. $v_\theta(r)$, so that the twisting magnetic fields are now sheared as well, $B_\theta(r)$.

The sheared magnetic field structure may be best illustrated by the analysis of the magnetic fields in terms of the local rotational transform $\iota(r,z)$ (Shafranov, 1970) and its associated so-called safety factor $q(r,z) = 2\pi/\iota = \bar{\iota}^1$ locally defined as

$$q(r,z) = \frac{rB_z}{RB_\theta(\mathbf{x})} ,$$

where $R = L_z/2\pi$. Since the twist is a function of z, the "rotational transform" and the safety factor are functions of z and are thus local (z) quantities. When q is, for example, 3 at $z = z_0$, the magnetic field is spiraling in the azimuthal direction with a pitch of $3L_z$. This would amount to a winding in the poloidal direction of the particular field line once while winding three times in the toroidal direction (in the periodicity of z) if this local $q = 3$ was held for all z. Such a local q is depicted in Fig. 1(a). From Shafranov's theory a strong kink instability is expected when q becomes less than unity. The result is in Fig. 1(b) for

the magnetic line. As the twisting continues, the magnetic field lines become more wrapped showing a wider area with $q < 1$ [Fig. 1(c)]. Figure 1(d) shows an distortion with azimuthal mode number $m = 1$ as exemplified by a crescent-shaped island and by a dipole structure.

Instead of causing the twisted field lines by twisting, one can study the isolated effects of the kink instability by starting a force-free equilibrium with field-aligned current ($\mathbf{j} \times \mathbf{B} = 0$) being sufficiently strong to begin with. Shown in Fig. 2 are two cases of such initializations, one with the current profile $j_z(r) \propto [1 + (kr)^2]^{-1}$, and the other with the Bessel functional current profile (Matsumoto and Tajima, 1994). In these particular cases the flux tube was emersed under the influence of a uniform gravity in the negative z-direction. We observe that the flux tube becomes unstable against the kink mode and the resultant field lines form a supercoil structure. Some portion of the supercoil rises due both to the kink and the gravitational buoyancy.

Shown in Fig. 3 is a case where we put in two point-like gravitational attractors as the arrows indicate and these gravitational objects have Keplerian disks with a bulge with their axis along the x-direction (Valinia and Tajima, 1994). The angular rotations of two disks are opposite and the magnetic field lines that penetrate through the disks are twisted as a result, as in the case of Fig. 1. As the twist gets stronger, the kink instability sets in as well as the evidence of the axial jet flows. This configuration and evolution may be thought of as a simplified version with only two clusters interacting one flux tube between them for the more complex N clusters interacting with a web of intercluster magnetic fields.

B. Reconnection of field lines and flux tubes

When shear flux surfaces are moved by the kink instability and one flux surface is squeezed against the other, magnetic field lines are pinched and reconnected around the X-point. This in fact happens in the kink mode associated with the action in the previous subsection. When the magnetic surface is totally reconnected and torn apart, a portion of plasma can be

expelled out into the exterior as seen in Fig. 1. In order to isolate the reconnection process of flux tubes or magnetic field lines, we illustrate the interaction of two flux tubes that are originally in force-free equilibrium similar to the one in Fig. 2(a). See Fig. 4(a). If two flux tubes carry currents that are parallel, while the axial magnetic fields are antiparallel, the magnetic helicity $\int_i \mathbf{A} \cdot \mathbf{B}\, dV$ of two tubes are antiparallel. Since two parallel currents are attractive and susceptible to the coalescence instability (Bhattacharjee *et al.* 1983), these two loops approach, as seen in Fig. 4(b). Similarly one can look at the case where the magnetic helicity of two loops are parallel. Although the classical tearing instability theory (White 1983) predicts no difference in reconnecting rates in these two cases, Figs. 4(a)–(f) along with Figs. 4(g)–(h) show that the antiparallel helicity case is much faster (and explosive) than the parallel helicity case. This effect has been predicted by Tajima (1981) and also seen in simulations (Leboeuf *et al.* 1982). Details have been analyzed by Tajima and Sakai (1989). The strong jet flows along the flux tubes after the reconnection are clearly seen in Fig. 4(d) for the antiparallel helicity reconnection. This antiparallel helicity reconnection can be many orders of magnitude faster than the tearing rate on the Sweet-Parker (1957–58) rate, and can be in the ball park of the Alfvén time scale, as seen in Fig. 4. An experimental verification of such a phenomenon has recently been found (Ono *et al.* 1993). Such a possibility of fast rate of reconnection is very significant, as astrophysical plasmas (particularly those of cosmology) are vast and the Lundquist number (the magnetic Reynolds number) tends to be huge and any intermediate time scale between the resistive and Alfvén time scales often tends to be too long for the age of the Universe or for its evolution.

III. Magnetically Constricted IGM Plasmas

We assume that global 'primordial' magnetic fields weave through clusters of galaxies. These magnetic fields are rapidly stretched, twisted, and braided by the violent relaxation of clusters of galaxies (Lynden-Bell 1969) in the supercluster gravitational potential. It is thus

natural that a substantial amount of the gravitational energy can be supplied to the magnetic energy at this stage. These intercluster fields tend to constrict the trapped gas, driving it to high densities and high temperatures. According to recent calculations of amplification of magnetic fields by the ABC dynamo (e.g. Galloway and Frisch 1986), the essence of the process of plasma motion of the violent relaxation is captured by the ABC dynamo, leading to chaotic flow, which in turn drive chaotic magnetic field lines and thus amplify them. The generated magnetic fields may exhibit chaotic and intermittent properties and attain filamentary and/or cellular structures, as will be discussed in Secs. V and VI.

As rapid relaxation (e.g. Taylor 1986) proceeds, we may apply a nearly force-free condition for such a magnetically constricted plasma;

$$\mathbf{J} \times \mathbf{B} + \nabla P \cong \text{const} . \tag{1}$$

Here P denotes the thermal pressure of the plasma. The kinetic temperature of a constricted plasma is hot enough to emit X-rays. Such X-ray 'brightening' is quite reminiscent of the phenomenon in the solar prominence, known as disparition brusques, in which disruption of filaments emitting X-rays driven by active motion of photospheric plasmas (see, e.g. Pneuman and Orrall 1986). Also related may be the X-ray brightening from the galactic ridge (Koyama *et al.* 1986) in the galactic disk, where the magnetic constriction may take place in a similar fashion. If we assumed a two-phase medium under pressure balance (see Guilbert and Fabian 1986), the space outside X-ray emitting hot plasmas should have been surrounded by a substantial amount of colder plasmas, requiring a huge mass in the colder component, or non-negligible distortion in CMBR by the hotter component.

It should be noted, however, that the (nearly) force-free condition does not necessary entail that the pressure balance holds in our model; i.e.

$$\left(\frac{B^2}{8\pi}\right) + P \neq \text{const} . \tag{2}$$

We now introduce a distribution function, $f(x,y,z)$, which is the probability to find a dense plasma at a certain point, (x,y,z). If we assume the completely random distribution of plasma inhomogeneities, $f(x,y,z) = f(x)f(y)f(z)$. The average of the probability function over a unit volume may be written as

$$\langle f(x,y,z)\rangle\, dV = \langle f(x)\rangle\, \langle f(y)\rangle\, \langle f(z)\rangle\, dV \equiv f\, dV\ . \tag{3}$$

Here brackets denote a volume average of physical quantities. This averaged probability function, f, is the volume-filling factor, and is expected to be much smaller than unity in our case, as we shall see below. In the following, we consider the situations where $f \ll 1$ keeping the total X-ray luminosity constant,

$$\int \mathcal{L}_X dV^p = \int \mathcal{L}_X^{\rm uni}\, dV^{\rm uni}\ , \tag{4}$$

where the superscript, uni, represents the value under the uniform assumption, and dV^p is the volume occupied by hot plasmas. Since $\mathcal{L}_X \propto n^2\sqrt{T}$ and $dV^p = f dV^{\rm uni}$, we have for the same temperature T, the density of X-ray emitting plasma is much higher than the uniform value:

$$n = f^{-1/2} n^{\rm uni}\ . \tag{5}$$

The Compton y parameter, which is proportional to $nT\,dz$, where dz is a length along the direction of the sight, is then reduced to

$$y = f^{1/2}\, y^{\rm uni}\ , \tag{6}$$

by a factor $f^{-1/2}(\gg 1)$ from the value obtained under the uniform assumption, because

$$dz^p = \langle f(x)f(y)\, f(z)dz\rangle = f\, dz\ . \tag{7}$$

Likewise, the total baryon density, Ω_B, is

$$\Omega_B \equiv \int n\, dV = f^{1/2}\, \Omega_B^{\rm uni}\ , \tag{8}$$

and becomes by a factor $f^{-1/2}$ smaller. It is suggested from COBE results that "the limits on y would limit the X-ray background to only 1/36 of the observed value" (Mather *et al.* 1990), indicating that $f \leq 10^{-3}$ in the present framework.

We know from the absence of absorption lines in QSO spectra that cold gas cannot be neutral (Gunn and Peterson 1965). The present model naturally satisfies this Gunn-Peterson test, because the present model need no cold dense gas for confinement of hot plasmas. It is, on the other hand, entirely possible that pockets of cold gas regions exist, as the thermal conduction is substantially reduced by the presence of magnetic fields, but still enough to ionize hydrogens in the cold gas.

IV. Heating of IGM Plasmas by Magnetic Fields

By the presence of magnetic fields, an efficient heating over a very large volume by a large amount is possible. This is because, in our model, no time is needed to form the network structure. For magnetical constriction to be possible, magnetic field strength is required to be at least

$$\frac{B^2}{4\pi} \geq n\,kT\ , \tag{9}$$

$$B \geq 2.5 \times 10^{-6}\ (\mathrm{Gauss}) \left(\frac{n}{10^{-6}\ \mathrm{cm}^{-3}}\right)^{1/2} \left(\frac{T}{300\,\mathrm{keV}}\right)^{1/2}\ . \tag{10}$$

Note that this field strength is local (to the hot plasma region) one, and is

$$B \sim f_B^{-1/2}\, B^{\mathrm{uni}}\ , \tag{11}$$

where f_B is the volume-filling factor for magnetic fields which is not necessarily the same as f for a plasma. For f_B of order 10^{-3}, the value obtained in Eq. (9) is consistent with the values of mean field strength of order 10^{-9} G derived by the measurements of the rotation measure (Fujimoto *et al.* 1971).

The heating provided by magnetic energy is

$$\mathcal{L}_X \sim \int \langle JE \rangle \, dV = \frac{1}{c} \int \frac{\partial B^2}{\partial t} \, dV \ , \tag{12}$$

$$\frac{\partial B}{\partial t} = \nabla \times (v \times B) + \eta \nabla^2 B \ . \tag{13}$$

The heating time in Eq. (12) is related to magnetic reconnection

$$\tau_{\rm rec} \sim R_m^{\epsilon - 1} \frac{\ell^2}{\eta_{\rm SH}} \ , \tag{14}$$

where ℓ is the characteristic spatial scale of the plasma, ϵ is determined by the dynamics of reconnection and relaxation. As we discussed in Sec. II, the parameter ϵ is generally $0 < \epsilon < 3/5$; $\epsilon = 0$ corresponds to the case of explosive reconnection (e.g. Petschek 1965; Tajima and Sakai 1989), whereas $\epsilon = 1/2$ is the case of Sweet-Parker-type (Parker 1957; Sweet 1958). The magnetic Reynolds number is

$$R_m \equiv \frac{1}{\nu_e} \left(\frac{v_A}{\ell} \right) \ , \tag{15}$$

where v_A is Alfvén velocity,

$$v_A = \frac{B}{\sqrt{4\pi n m_p}} \ , \tag{16}$$

ν_e is the collision frequency (T in eV),

$$\nu_e = 3 \times 10^{-6} \, n (\ln \Lambda) T^{-3/2} \ , \tag{17}$$

and the Spitzer-Härm conductivity is

$$\eta_{\rm SH} = 7 \times 10^6 \, \frac{\ln \Lambda}{T^{3/2}} \ . \tag{18}$$

For relevant values and $\epsilon = 0$, for example, we find

$$\mathcal{L}_X \sim 3 \times 10^{55} \, \frac{1}{\tau_{\rm rec}} \left(\frac{B}{10^{-6} \, G} \right)^2 \left(\frac{L}{10^{25} \, {\rm cm}} \right)^3 \ . \tag{19}$$

where L is the supercluster size. From the observed energy requirement (Guilbert and Fabian 1986) $\mathcal{L}_X \sim 10^{62}/\tau_{\rm cool}$, where $\gamma_{\rm cool}$ is the radiative cooling rate. We therefore get

$$\frac{\tau_{\rm rec}}{\tau_{\rm cool}} \simeq 10^{-6} \left(\frac{B}{10^{-6}\,G}\right)^2 \left(\frac{L}{10^{25}\,{\rm cm}}\right)^3 . \tag{20}$$

Equations (14) together with (20) determine the length scale on which reconnection takes place:

$$\ell = \left[10^{14}\,\frac{\eta_{\rm SH}}{\nu_e^{1-\epsilon}} \left(\frac{B}{10^{-6}\,G}\right)^2 v_A^{1-\epsilon}\right]^{1/3-\epsilon} . \tag{21}$$

This reduces, for example for $\epsilon = 0$, to $\ell \propto n^{-1/6} B$, and takes the value of $\ell \sim 10^{11-14}\,{\rm cm}$ for $\frac{1}{2} > \epsilon > 0$ with the cooling time of $10^{20}\,{\rm s}$ with $B({\rm local}) \sim 1\mu\,G$. This is not unreasonable if B is highly intermittent and turbulent as widely suspected of chaotic field lines.

We introduced a new picture for the IGM that removes the difficulties of the existing models facing the observed X-ray emissivities, the distortion in CMBR, and the total baryon number. It is demonstrated that the cosmic X-ray background is accounted for by hot plasmas constricted by weaving magnetic fields, driven by the violent relaxation of clusters of galaxies. This mechanism naturally explains the epoch of the cosmic X-ray background, as it is related to the epoch of violent gravitational relaxation; otherwise the X-ray spectrum would be much wider. The effects of such magnetic fields are that, with the known X-ray emissivity, (i) the Compton influence on the CMBR (Compton y parameter) and the total baryon density (Ω_B) are both reduced by a factor $f^{-1/2} (\gg 1)$; (ii) there exists enough magnetic energies to account for X-ray emission and the necessary heating rate determines the spatial scales of the fine structure of the chaotic magnetic fields.

V. The ABC Dynamo

We now return to the problem of how the primordial large-scale magnetic fields and their structure may have been formed, which have contributed to the kind of fields needed for the cosmic X-ray background radiation considered in previous sections. Recently there has been

a renewed effort to explain the existence of the large-scale structures in the universe. New observations indicate structures on the largest scales (Saunders *et al.* 1991, Broadhurst, *et al.* 1990; de Lapparent, *et al.* 1989), as well as an ever-decreasing limit on the non-uniformity of the cosmic microwave background at the time that matter and radiation decoupled (Mather *et al.* 1990; Smoot *et al.* 1992). It is well known that for given matter fluctuations compatible with this low level of electromagnetic fluctuations, there has been too little time since the recombination to allow for the formation of observed galactic and other structures. The current "cold dark matter" theory tries to answer this difficulty. It may be possible to introduce additional elements to consider that (i) the radiation epoch in the primordial universe was crucial in preparing for the formation of large structures via magnetic interactions, and (ii) the magnetic structures involved were isothermal in nature and so did not leave an imprint on the high-frequency blackbody spectrum.

During the period from 10^{-2} to 10^{13} second after the big bang, the universe consisted primarily of an expanding electron-(positron)-proton plasma, and the electromagnetic interaction was the dominant force. Thus this period may be called the "radiation epoch" or "plasma epoch." If fluctuations led to the growth of seed magnetic fields during this time, then the resulting fields may have had a significant effect on the distribution of matter. There have been several works on the magnetic field evolution in the early universe (Harrison, 1970, Sato *et al.* 1971; Baierlein, 1978).

Investigations such as Harrison's have assumed primordial turbulence with nonzero vorticity. However, the assumption of the presence of turbulent flows seems to find less supporters these days because the presence of flow and the observed homogeneity in the 3K microwave background are believed to be incompatible (Rees, 1987). On the other hand, it is unclear whether the incompressible (or vortical) flow motion of low- or zero-frequency would leave an observable imprint on the cosmic background. The coupling of photons with adiabatic perturbations such as sound motions and that with nonadiabatic vortical motions

are quite different. One of the major differences is that the latter need not incur density perturbations, and as such it is more difficult for nonadiabatic vortical motions to couple to photons (Tajima and Taniuti, 1990). It is in fact quite natural to take the incompressible mode for the very large-scale slow motion that we are interested in. Furthermore, it has recently been shown (Tajima *et al.* 1992a) that in the early epoch of the radiation era it is possible that the nearly zero-frequency magnetic fluctuations associated with a plasma in an (even perfect) thermal equilibrium can be substantial based on the rigorous theory of the fluctuation-dissipation theorem (Sitenko, 1967). The nearly static magnetic fluctuations can couple with the plasma, thus creating density and velocity fluctuations, while the high frequency photons couple more weakly with the plasma. The presence of such magnetic, density and velocity fluctuations, albeit with small-scale seed fields, could influence the subsequent evolution of spatially larger scales of fluctuations. Furthermore fluctuations with size $\lambda > ct$ (the horizon) are certainly not in thermal equilibrium and thus could give rise to non-equilibrium noise. These magnetic fluctuations decayed only slowly in time after they entered the horizon, with the diffusive relaxation time scale $t_{\rm dif} \approx \omega_p^2 \lambda^2 / \nu c^2$, where ν is the collision frequency. If $t_{\rm dif}$ is longer than the interval between the entrance time into the horizon and the exit time (i.e., the recombination time), such magnetic fluctuations were unable to reach thermal equilibrium; see Fig. 5. (The velocity fluctuations decay faster due to viscosity than magnetic fluctuations.) This provides large-scale seed fields. It is tempting to consider (Fujimoto, 1990) such seed fields that were amplified as a candidate for creating recently discovered large-scale structures.

In this paper we investigate, through a very simple model, the characteristic morphology and strength of the magnetic fields that may result from dynamo action in an expanding highly conducting medium. This will provide some qualitative understanding of the interplay between the exponentiation of the field that can result from an incompressible chaotic flow, and the effects of the expansion of the medium. Here we are concerned with large-scale

magnetic fields. The relation of microscopic fields (as discussed in Tajima *et al.* 1992a) to such macroscopic fields is important (Tajima *et al.* 1992b).

In addition to the epoch prior to recombination the epoch after recombination may also be relevant. After the recombination most constituent matter becomes charge neutral and the main interactive force becomes gravitational rather than electromagnetic. It is known, however, that there exists very hot tenuous plasma in the intergalactic (or intersupercluster) space (Giovannini *et al.* 1990). Such hot plasma may be of recent creation as we discussed in Sec. III; on the other hand, it may well be of primordial nature (i.e., around the time of recombination). For example, the post-recombination violent relaxation of gravitationally unstable neutral matter can twist and stretch pre-existing magnetic fields that have been created prior to recombination. Matter may be heated by this stretching and twisting, thus creating and sustaining hot tenuous plasmas on the surface of denser matter and beyond. In addition, even without such, the ionization rate immediately after the recombination did not go below 10^{-6}. Such plasmas provide an alternative medium for the dynamo action of cosmological magnetic fields as well as galactic magnetic fields. Such magnetic fields may provide the necessary energy for X-ray emissions known as the cosmic X-ray background (e.g. Guilbert and Fabian, 1986). The dynamo action after the recombination was investigated by many others, including Ruzmaikin and Sokoloff (1977), Zweibel (1988), and Anderson and Kulsrud (1991).

There do appear to exist cosmic magnetic fields of order 10^{-6} G (see Norman, 1990 and references therein). These recent works tend to support the view that the galactic dynamo has not had time to generate the observed fields. Such findings seem to suggest that they evolved either during the plasma epoch or soon after recombination as described above.

In what follows we are interested in the cosmological dynamo as opposed to the galactic dynamo. We are interested in general morphologies and other global characteristics of dynamo action in highly conducting plasmas with expanding background. In the cosmological

dynamo, we are concerned about large-scale magnetic fields whose size may be relevant to galaxy formation. In this scale the magnetic Reynolds number is extremely large. If the dynamo action takes place, it has to be effective in this nearly dissipationless situation. On this large spatial scale the fast sound time scale can be coarse-grained. Thus we are dealing only with the vortical component of velocities.

As a simple model, we adapt one used by Finn and Ott (1988) as a example of a steady fast dynamo. A fast dynamo refers to a dynamo in which magnetic field amplification can take place even in the limit where resistivity $\gamma \to 0$. They used the "ABC map," which is the discrete-time version of the 3D, incompressible, periodic "ABC flow" (named for Arnold, Beltrami, and Childress). The ABC flow, given by the velocity field

$$\begin{aligned} v_x &= A\,\sin(z) + C\,\cos(y) \\ v_y &= B\,\sin(x) + A\,\cos(z) \\ v_z &= C\,\sin(y) + B\,\cos(x) \qquad (\text{mod } 2\pi)\ , \end{aligned} \tag{22}$$

is a simple steady-state solution of the Euler equation describing incompressible flows:

$$\frac{\partial \mathbf{v}}{\partial t} + \omega \times \mathbf{v} = -\nabla\left(\frac{p+v^2}{2}\right)\ , \tag{23}$$

where the vorticity $\omega \equiv \nabla \times \mathbf{v}$ and $\nabla \cdot \mathbf{v} = 0$. It is possible to generalize (22) to include arbitrary spatial scales other than 2π by regarding A,B,C as specific Fourier coefficients associated with such spatial scales.

Arnold suggested, and subsequent workers have confirmed, that this flow exhibits chaotic streamlines. When the flow is chaotic, adjacent fluid elements separate exponentially (the so-called Lyapunov exponentiation). In the limit $R_m \to \infty$ the magnetic field lines are "frozen in" to the fluid elements. The stretching of fluid elements leads to exponential collapse of the area through which magnetic flux penetrates and therefore to exponential enhancement

of magnetic field intensity in the fluid. Since streamlines lie on surfaces where $p + v^2/2 =$ constant (from Eq. (23), space-filling chaotic streamlines can exist only in the neighborhoods where

$$\nabla \left(\frac{p + v^2}{2} \right) = \omega \times \mathbf{v} = 0 \, . \tag{24}$$

This defines the "Beltrami property":

$$\omega \equiv \nabla \times \mathbf{v} = \Lambda \mathbf{v} \, , \tag{25}$$

where Λ is a function of the streamline. In special cases Λ can be constant in the entire space. This arises, for example, when the flow is globally chaotic. A similar case for magnetic turbulence was postulated by Taylor (1978) for a toroidal confinement machine. The ABC flow satisfied the Beltrami property for the simplest case $\Lambda = 1$.

The structure of the ABC flow has been studied in detail by Dombre *et al.* (1986), who demonstrated the existence of an intricate mixture of regular and chaotic streamlines. Dynamo action for the ABC flow was studied by Galloway and Frisch (1986), who numerically integrated the induction equation

$$\frac{\partial \mathbf{B}}{\partial t} + \mathbf{v} \cdot \nabla \mathbf{B} = \mathbf{B} \cdot \nabla \mathbf{v} + \frac{1}{R_m} \nabla^2 \mathbf{B} \tag{26}$$

for finite values of the magnetic Reynolds number $R_m \equiv v_0 \lambda / \gamma$. (Here v_0 is the characteristic velocity, λ is the characteristic length scale, and γ is the resistivity.) They observed exponential growth of initial magnetic fields for certain ranges of R_m. The field growth was found to be concentrated in the regions of chaotic streamlines, as expected from the above discussion.

The mapping, which gives the position of fluid elements at discrete times, can be obtained by a finite-differencing or strobing of the flow, yielding

$$x_{n+1} = x_n + A \sin(z_n) + C \cos(y_n) \, ,$$

$$y_{n+1} = y_n + B\,\sin(x_{n+1}) + A\,\cos(z_n)\ , \tag{27}$$

$$z_{n+1} = z_n + C\,\sin(y_{n+1}) + B\,\cos(x_{n+1}) \qquad (\mathrm{mod}\ 2\pi)\ .$$

Here the subscripts refer to the time, and the timestep has been absorbed into the coefficients A,B,C. The map is a good approximation to the flow for A,B,C$\ll 1$. It has the property that the coordinate transformation between points in time is symplectic; it therefore exactly preserves the incompressible nature of the flow. The structure of the streamlines and the dependence on the coefficients has been studied by Feingold *et al.* (1988). Here we will indicate briefly the topology of the mapping for values of A,B,C that will be of interest to us.

A useful tool for understanding the topology of a three-dimensional flow is the Poincáre surface-of-section. This consists of plotting intersections of trajectories with some two-dimensional surface in space. In the case of the mapping, since an exact intersection with the plane will rarely occur, we must instead plot intersections with a thin slice of the space. In Figs. 6(a)–(c) we show the section $0 \le z \le 0.01$ for the cases

$$\{A = 0.001,\ B = C = 1.0\}$$

$$\{A = B = C = 0.30\}$$

$$\{A = B = C = 0.03\}$$

respectively. For each plot we started initial conditions at several different locations, and iterated 50,000 times. In the first case the periodicity cube contains mainly tubes of regular motion oriented in the z-direction, separated by thin strips of chaotic motion. In the other two cases we see a complex mixture of regular surfaces and chaotic regions, with the behavior being confined to smaller portions of the space for the smaller value of A,B,C. (For both of these cases the structure is identical in the other two dimensions.) Figure 6(d) is a projection

of x and y values for the same parameters as in Fig. 6(c); here we plot all points rather than those falling in a slice of the space. We will refer back to these figures in Sec. VI of the paper.

Finn and Ott used the ABC map to study dynamo action in the limit $R_m \to \infty$. In this limit the induction equation becomes

$$\frac{d\mathbf{B}}{dt} \equiv \frac{\partial \mathbf{B}}{\partial t} + \mathbf{v} \cdot \nabla \mathbf{B} = \mathbf{B} \cdot \nabla \mathbf{v} \ . \tag{28}$$

The fluid equation has the characteristics $\frac{d\mathbf{x}}{dt} = \mathbf{v}$, and an infinitesimal displacement $\delta\mathbf{x}$ satisfies the equation

$$\frac{d(\delta \mathbf{x})}{dt} = \delta \mathbf{x} \cdot \nabla \mathbf{v} \ , \tag{29}$$

which is the same equation obeyed by $\mathbf{B}$. Thus we can follow the evolution of this frozen-in field by iterating the map which gives the motion of the fluid elements. In the studies by Finn and Ott the resulting stretching and folding of the field lines was shown (for A,B,C= 1.5) to result in exponential growth of magnetic flux, as well as increasingly fine-scaled structure.

Their basic algorithm, which we will use, was as follows. First a set of points (for example a plane) was chosen on which they wanted to follow the evolution of the initial field. To observe the evolution of the field after n time steps, they first iterated the map backward n steps in time to find the set of fluid elements that would end up at the locations of interest. The magnetic field at time n was then taken to be given by the following linearized mapping:

$$\mathbf{B}(\mathbf{x}(n)) = \mathbf{J}(\mathbf{x}_{n-1}) \cdot \mathbf{J}(\mathbf{x}_{n-2}) \cdots \mathbf{J}(\mathbf{x}_1) \cdot \mathbf{J}(\mathbf{x}_0) \cdot \mathbf{B}(0) \ , \tag{30}$$

where $\mathbf{J}(\mathbf{x})$ is the Jacobian matrix for the map. We are interested primarily in the case where A,B,C are sufficiently less than unity so that the mapping (27) is a good finite difference representation of the differential equations (22).

Our work has used an adaptation of this model which includes effects due to expansion of the medium. One of these effects is the decay of the velocity field. If the period we investigate

is in the radiation epoch, then from standard big bang theory (e.g. Misner *et al.* 1970) we take the expansion of the universe to be given by $a = a_0(t/t_0)^{1/2}$ where a is the characteristic length scale, and the subscripts refer to the present time. The velocity fluctuations are expected to decay in time. For example, we may take the characteristic velocity to go like $v \propto 1/a$ if we assume that the peculiar velocity in the ϕ-direction is $v_\phi \equiv (\Omega \times \mathbf{r})_\phi =$ constant (does not decay due to the cosmic expansion). Then $v \propto t^{-1/2}$. A viscous damping is also possible. For times after the recombination we would take $a = a_0(t/t_0)^{2/3}$. In our mapping representation, this is represented as a "time" dependence of the coefficients:

$$A = \frac{A_0}{[\alpha(n_0 + n)]^{1/2}} , \qquad \text{etc.} \tag{31}$$

Here n is the number of iterations (i.e., the time measured in characteristic "dynamo times"), and α is the ratio of the characteristic expansion time to the dynamo time. n_0 is the initial time of dynamo action. (In the work presented here we used $\alpha = 1, n_0 = 1$.)

This time dependence of the coefficients means that the structure of the velocity field will change in time. For A,B,C$\geq$ 1, nearly all streamlines are chaotic, and we can have flux growth throughout the space. On the other hand, when A,B,C$\ll$ 1, then most of the space contains regular motion, and we would expect the strong flux growth to be confined to small regions. So we expect that as time goes on, our velocity field will become more regular and structured, and the regions of strong magnetic field growth will become concentrated into structures of relatively small volume.

The other effect included is the decay of magnetic field strength due to the expansion of the medium. When dynamo action is absent, this follows from flux conservation, since we would then have

$$\text{flux} \equiv \Phi \equiv Ba^2 = \text{ constant, therefore}$$

$$B \propto \frac{1}{a^2} \propto \frac{1}{t} . \tag{32}$$

In our model this is incorporated by dividing the magnetic field at time n by the factor $\alpha(n_0 + n)$.

A useful parameter for quantifying the field growth is the plasma beta: $\beta \equiv 8\pi P/B^2 = 8\pi nT/B^2$. For isentropic expansion, we have $Ta =$ constant, thus $T \propto 1/a$. Using $n \propto 1/a^3$ and $B \propto 1/a^2$, we have $\beta =$ constant. This is the case for simple cosmic expansion with constant magnetic flux. However, if dynamo action leads to flux growth, then β will decrease.

VI. Numerical Results of the ABC Dynamo

Using the model described above, we have carried out a series of numerical experiments to study the growth of magnetic fields in an expanding medium. In most of the runs presented here we kept A=B=C at all times. As A,B,C decrease with time, the topology of the streamlines will go through phases as indicated in Figs. 6(b)–(c). As the ABC flow is not a general flow this imposed a particular structure on the velocity field as a function of time. Within the limits of this imposed structure, we wanted to determine whether local magnetic fields could be maintained against the effects of expansion, to see what structures would occur, and to see how the field behavior depended on the parameters of the model.

We examined the evolution of the magnetic field energy both on a plane ($z = 0$) in space and in the whole periodicity cube ($2\pi \times 2\pi \times 2\pi$). We work with a grid of ninety-nine points in each direction, and in all runs so far assume an initially uniform magnetic field in the z-direction of strength $B_0 = 1$ in arbitrary units.

In Fig. 7 we plot the field energy B^2 on the $z = 0$ plane at various times, for $A_0 = B_0 = C_0 = 0.3$ and $\alpha = 1$. (A logarithmic scale is used.) As shown by Finn and Ott, the magnetic field develops increasingly fine-scaled structure as time goes on, with strong, oppositely-directed fields on nearby grid points. We have done a coarse-graining to eliminate some of this fine structure for illustration purpose. The plots of Fig. 6 are on a grid of 33×33 points covering the $2\pi \times 2\pi$ square. The magnetic field at each of these points was obtained

by summing over nine points from the original 99×99 grid.

In Fig. 7(a) we see that the field decays on most of the plane, but is maintaining itself or growing in certain regions.

A three-dimensional view of this structure is given in Fig. 8. Here we plot surfaces in the periodicity cube within which the magnetic energy is greater than 3% and 25% of its original value, at time $n = 50$. The high-field regions are concentrated in domains where streamlines are strongly chaotic. In regions of non-chaotic flow the magnetic field strength falls to much smaller values.

As stated before, one measure of field growth is the decrease in the plasma beta. In Figs. 9 and 10 we have plotted both field energy and β vs. time for the central point of the 33×33 grid. Figure 9 corresponds to the parameters $A_0 = 0.001$, $B_0 = C_0 = 1.0$; in this case the central grid point lies in a region of regular flow (see Fig. 6), and field growth would not be expected. Indeed we see that β remains constant. Figure 10 corresponds to $A_0 = B_0 = C_0 = 0.3$; in this case the central point lies in a region of chaotic flow [see Figs. 6(b)–(c)] where the field is growing (as seen in Fig. 7). Here we see large fluctuations in both field energy and in β, but over long times the energy maintains itself and β decreases.

Figures 11–12 show corresponding output for $A_0 = B_0 = C_0 = 1.0$. In this case we initially have chaotic streamlines throughout the whole space; as time progresses we obtain structures as we have seen earlier. (Of course for large A,B,C the mapping will not be a good representation of the original flow, but is still an example of a highly chaotic incompressible flow.) The effect of increasing the coefficients (and therefore filling more of the space with chaotic streamlines) appears to be a simple increase in the frequency of fluctuations of the magnetic energy about a roughly constant mean value. (This held true for a variety of cases that we examined.) The field strength does not exhibit exponentiation as it would in a non-expanding medium, but in each case it seems to maintain itself against the effects of the expansion and the decay in the velocity field.

We have presented a considerably simplified model of dynamo action in the primordial universe. In this work we retained only a few characteristics of the physical situation, including the large-scale character, the highly conducting nature, the slow time scale in terms of incompressibility of the model, and cosmic expansion. Under a certain set of fairly general conditions we computationally observe cellular pattern formation of magnetic fields (as seen in Fig. 8). Such magnetic fields may have left an imprint on the primordial universe.

This dynamo model may be applicable both before and after the recombination time with proper interpretation. In the epoch prior to recombination ($t \sim 10^3$ sec) the universe is basically a highly conducting plasma. As has been shown, this plasma even in perfect thermal equilibrium contains substantial (nearly) zero-frequency magnetic fields, which can act as seed fields for dynamo action. Likewise, it contains velocity fluctuations of low frequency (either of thermal noise origin or from the horizon crossing) which can act as amplifiers of the fields. The question of whether the fields can detach from the thermal equilibrium state and hydrodynamically evolve through Eqs. (28) and (29) is a profound one and we leave this for future investigation (Cable and Tajima 1994). In the epoch after recombination the universe may generate a tenuous plasma through violent relaxation, with shredded primordial magnetic fields acting as a heating agent. The velocity fields generated by relaxation may yield the dynamo action. Then once again the ABC model may be applied.

In either case our interest is in the global morphology: the observed cellular structure formation, which could have left an imprint on the plasma density in the early universe. Certainly these models are quite simplistic for a realistic model of cosmology; in the future one needs to determine cosmological implications in more detail.

I appreciate contributions by Drs. S. Mineshige and Matsumoto, and Mr. C. Kueney and Ms. A. Valinia's computational help. This work was supported by NSF ATM-91-13576 and the U.S. Dept. of Energy contract #DE-FG05-80ET-53088.

References

Anderson, S., and R.M. Kulsrud, private communication (1991).

Baierlein, R. 1978, Mon. Not. R. Astr. Soc., **184**, 843.

Balbus, S.A., and J.F. Hawley 1992, Ap.J., **400**, 610.

Bhattacharjee, A., F. Brunel, and T. Tajima 1983, Phys. Fluids, **26**, 3332.

Broadhurst, T.J., R.S. Ellis, D.C. Koo, and A.S. Szalay 1990, Nature, **343**, 1726.

Cable, S., and T. Tajima 1994, Univ. of Texas preprint.

De Lapparent, V., M.J. Geller, and J.P. Huchra 1989, Ap.J., **343**, 1.

Dombre, T., U. Frisch, J.M. Greene, H. Henon, A. Mehr, and A.M. Soward 1986, J. Fluid Mech., **167**, 353.

Feingold, M., L.P. Kadanoff, and O. Piro 1988, J. Stat. Phys., **50**, 529.

Finn, J.M., and E. Ott 1988, Phys. Fluids, **31**, 2992.

Field, G.B., and S.C. Perrenod 1977, Ap.J., **215**, 717.

Fujimoto, M. 1990, Publ. Astr. Soc. Japan, **42**, L39.

Fujimoto, M., Y. Sofue, and K. Kawabata 1971, Prog. Theor. Phys. Suppl., **49**, 181.

Galloway, D., and U. Frisch 1986, Geophys. Astrophys. Fluid Dyn., **36**, 53.

Giovannini, G., K.-T. Kim, P.P. Kronberg, and T. Venturi 1990, in *Galactic and Intergalactic Magnetic Fields*, ed. R. Beck *et al.* (Dordrecht: Kluwer Academic Press), 492.

Guilbert, P.W., and A.C. Fabian 1986, Mon. Not. R. Astr. Soc., **220**, 439.

Gunn, J.E., and B.A. Peterson 1965, Ap.J., **142**, 1633.

Harrison, E.R. 1970, Phys. Rev. D, 1, 2726.

Kim, K.-T, P.C. Tribble, and P.P. Kronberg 1991, Ap.J., **379**, 80.

Koyama, K., K. Makishima, Y. Tanaka, and H. Tsunei 1986, Publ. Astron. Soc. Jpn. **38**,121.

Kueny, C. and T. Tajima 1991, Univ. of Texas at Austin preprint.

Lahav, O., Loeb, A., and McKee, C.F. 1990, Ap.J., **329**, L9.

Leboeuf, J.N., T. Tajima, and J.M. Dawson 1982, Phys. Fluids, **25**, 784.

Lynden-Bell, D. 1967, MNRAS, **136**, 101.

Mather, J.C., E. Cheng, R. Eplee, R. Isaacman, S. Meyer, R. Schafer, R. Weiss, E. Wright, C. Bennett, N. Boggess, E. Dwek, S. Gulkis, M. Hauser, M. Janssen, T. Kelsall, P. Lubin, S. Moseley, T. Murdock, R. Silverberg, G.F. Smoot, and D. Wilkinson 1990, Ap.J., **354**, L37.

Matsumoto, R., and T. Tajima 1992, Univ. of Texas preprint.

Misner, C.W., K.S. Thorne, and J.A. Wheeler *Gravitation*, (W.H. Freeman, San Francisco, 1970), p. 764.

Norman, C.A. 1990, in *Confrontation between Theories and Observations in Cosmology: Present Status and Future Programmes*, ed. J. Audouze and F. Melchiorri (North-Holland, 1990), p. 29.

Parker, E.N. 1957, J. Geophys. Res., **62**, 509.

Petschek, H.E. 1965, in AAS-NASA Symposium on the Physics of Solar Flares, ed. W.N. Hess (NASA SP-50) (NASA, Washington, D.C.), 425.

Pnewman, G.W., and F.Q. Orrall 1986, in *Physics of the Sun*, eds. P.A. Sturrock, T.E. Holzer, D.M. Mihalas, and R.K. Ulrich (Dordrecht: Reidel), 111.

Rees, M., in *The Very Early Universe*, eds. G.W. Gibbons, S.W. Hawking, and S.T.C. Siklos (Cambridge Univ. Press, 1987), p. 29.

Ruzmaikin, A.A., and D.D. Sokoloff 1977, Astrofizika, **13**, 95.

Sato, H., T. Matsuda, and H. Takeda 1971, Prog. Theor. Phys. Suppl., **49**, 11.

Saunders, W., C. Frenk, M. Rowan-Robinson, G. Efstathiou, A. Lawrence, N.

Kaiser, R. Ellis, J. Crawford, X. Xia, and I. Perry 1991, Nature, **349**, 32.

Shafranov, V.D. *Reviews of Plasma Physics* (Consultants Bureau, NY, 1970) Vol. 2, p. 103.

Sitenko, A.G., *Electromagnetic Fluctuations in Plasmas* (Academic Press, New York, 1967).

Smoot, G.F. *et al.* 1992, Ap.J. **396**, L1.

Steinolfson, R.S., and T. Tajima 1987, Ap.J. ,**322**, 503.

Sunyaev, R.A., and Ya.B. Zeldovich 1972, A&A, **20**, 189.

Sweet, P.A. 1958, in Electromagnetic Phenomena in Cosmic Physics, IAU Symp. No. 6 ed. B. Lehnert (Cambridge: Cambridge Univ. Press), 123.

Tajima, T., in *Fusion Energy* (ICTP, Trieste, 1981) p. 403.

Tajima, T., and J.-I. Sakai 1989, Sov. J. Plasma Phys., **15**, 519.

Tajima, T., and S. Mineshige 1991, Univ. of Texas at Austin preprint.

Tajima, T., K. Shibata, S Cable, and R.M. Kulsrud 1992a, Ap.J., **390**, 309.

Tajima, T., S. Cable, and R.M. Kulsrud 1992b, Phys. Fluids B, **4**, 2338.

Tajima, T., and T. Taniuti 1990, Phys. Rev. A, **42**, 3587.

Taylor, J.B. 1978, Phys. Rev. Lett., **33**, 1139.

Taylor, J.B., and E.L. Wright 1989, Ap.J., **339**, 619.

Taylor, J.B. 1986, Rev. Mod. Phys., **58**, 741.

Tribble, P.C. 1991, MNRAS, **253**, 147.

Valentijn, E.A. 1990, Nature, **346**, 153.

Valinia, A., and T. Tajima 1994, to be published.

White, R.B., in *Handbook for Plasma Physics* (North-Holland, Amsterdam, 1983) Vol. 1.

Zaidman, E., and T. Tajima 1989, Ap.J., **338**, 1139.

Zweibel, E.G. 1988, Ap.J., **329**, L1.

Figure Captions

1. The q profiles (a) and (c) and twisted magnetic field lines (b) and (d) with shear. (a) and (b) in early time and (c) and (d) after kink sets in.

2. The kink mode evolution of twisted (current-carrying) magnetic flux tube which was originally in force-free equilibria.

3. The flux tube evolution that is being twisted by differentially counter-rotating two disks with compact gravitational centers. The density (a), the field lines (b), and the jet flows out of the disk centers (c).

4. Coalescence of two flux tubes with antiparallel [(a)–(f)] or parallel [(g)–(h)] magnetic helicity.

5. Small-scale and large-scale perturbations during the radiation epoch ($10^{-2} < t < 10^{13}$ sec) are shown as a function of time. The small-scale fluctuations could be amplified in amplitude and size. The entering nonequilibrium large scales are indicated by two lines, one corresponding to the present galaxy size and the other to the largest obseved structures.

6. Plots of x and y values of fluid elements forf various initial conditions for the mapping of Eqs. (6); (a) $A = 0.001, B = C = 1.0$, $0 \leq z \leq 0.01$, $n = 50,000$; (b) $A = B = C = 0.30$, $0 \leq z \leq 0.01$, $n = 50,000$; (c) $A = B = C = 0.03$, $0 \leq z \leq 0.01$, $n = 50,000$; (d) $A = B = C = 0.03$, all z, $n \sim 2,000$.

7. Magnetic field energy as a function of x and y on the $z = 0$ plane in an expanding medium with $A_0 = B_0 = C_0 = 0.3$; the magnetic field at each point of this 33×33

grid is the sum over nine points of the original 99×99 grid; (a) $n = 0$; (b) $n = 50$; (c) $n = 100$.

8. Surfaces in the periodicity cube ($0 \leq x, y, z \leq 2\pi$) for which the magnetic field energy is greater than (a) 3% and (b) 25% of its original value for $A_0 = B_0 = C_0 = 0.3, n = 50$.

9. (a) Magnetic energy vs. time at the center of the $z = 0$ plane for $A_0 = 0.001, B_0 = C_0 = 1.0$; (b) plasma beta vs. time for the same case.

10. (a) Magnetic energy vs. time at the center of the $z = 0$ plane for $A_0 = B_0 = C_0 = 0.3$; (b) plasma beta vs. time for the same case.

11. Magnetic field energy as a function of x and y on the $z = 0$ plane for $A_0 = B_0 = C_0 = 1.0$; (a) $n = 50$; (b) $n = 100$.

12. (a) Magnetic energy vs. time at the center of the $z = 0$ plane for $A_0 = B_0 = C_0 = 1.0$; (b) plasma beta vs. time for the same case.

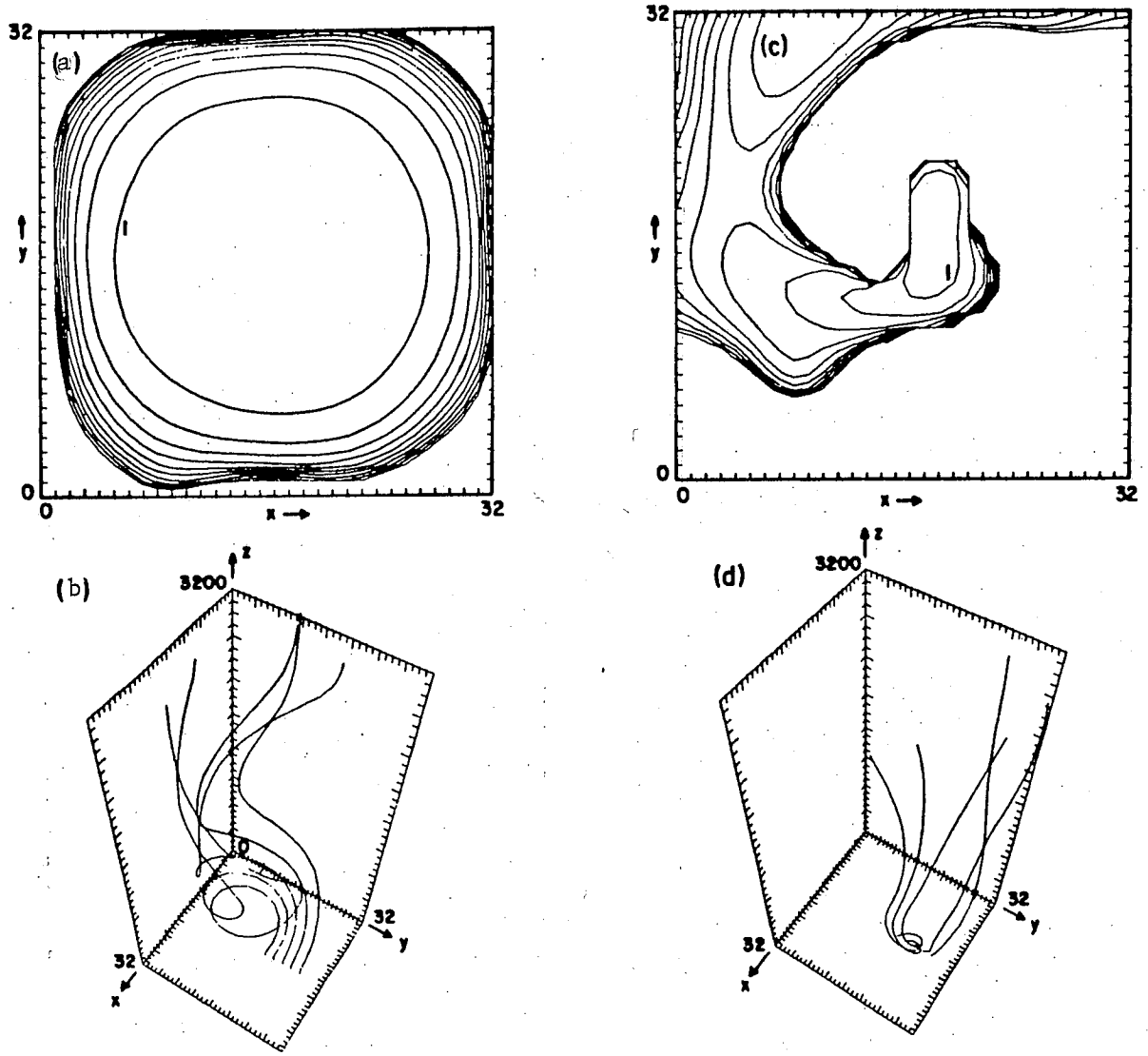

Fig. 1

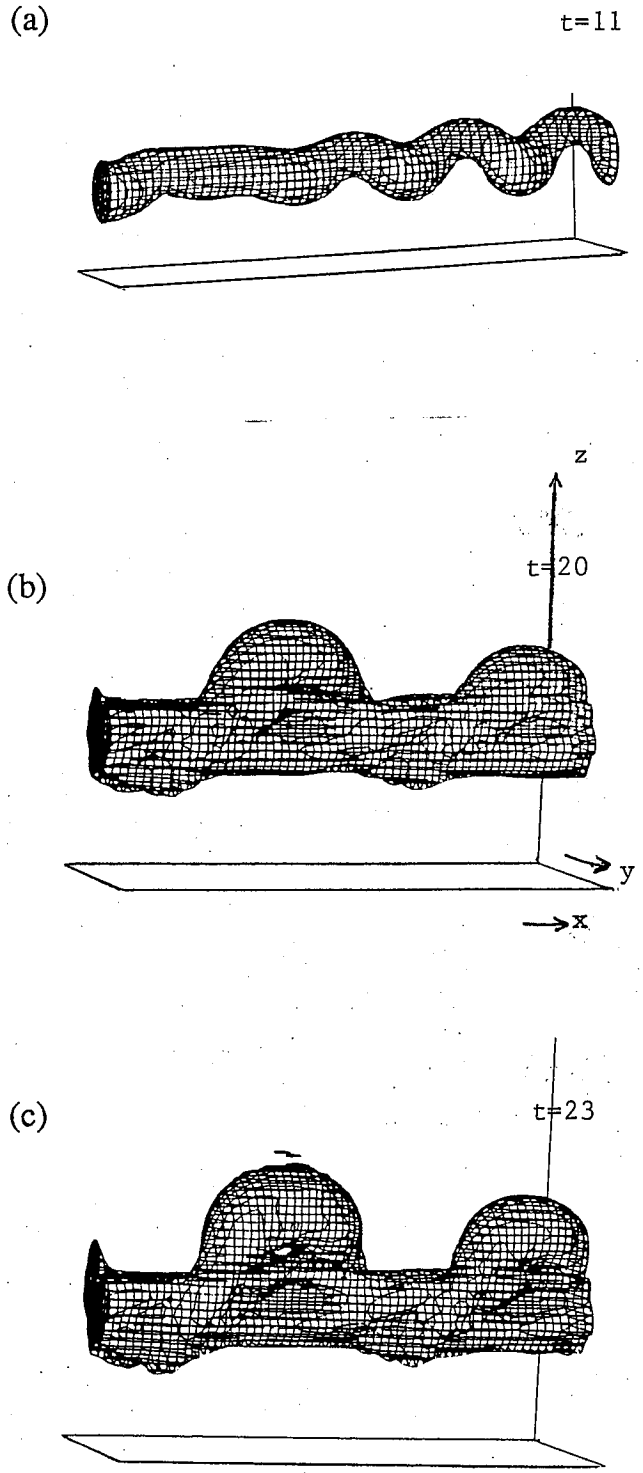

Fig. 2

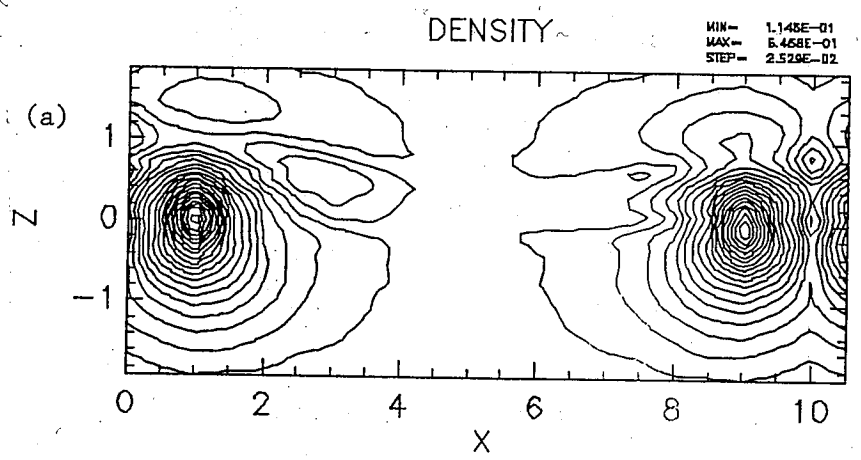
DENSITY
MIN= 1.145E-01
MAX= 5.458E-01
STEP= 2.529E-02
(a)
Z
1
0
−1
0
2
4
6
8
10
X

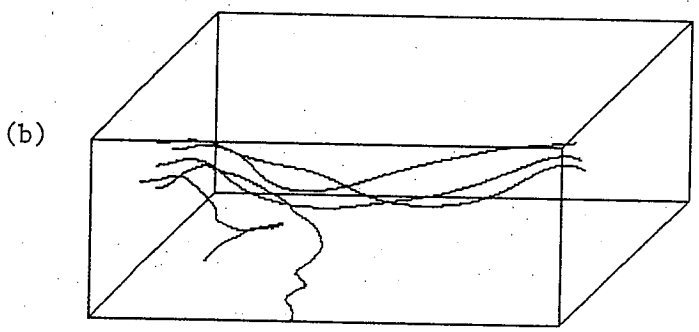
(b)

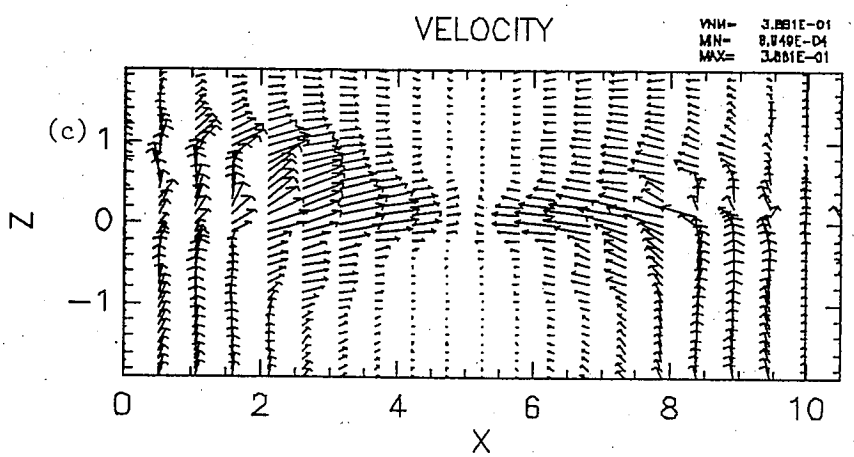
VELOCITY
VMN= 3.881E-01
MIN= 8.049E-04
MAX= 3.881E-01
(c)
Z
1
0
−1
0
2
4
6
8
10
X

Fig. 3

(a)

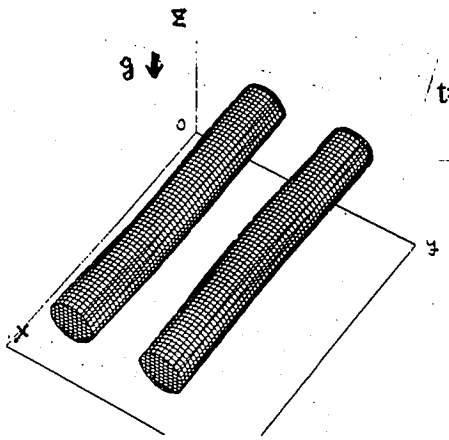

t=0

antiparallel helicity

(b)

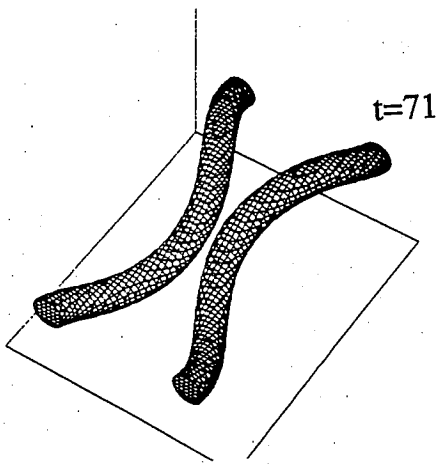

t=71 d/v_A

(c)

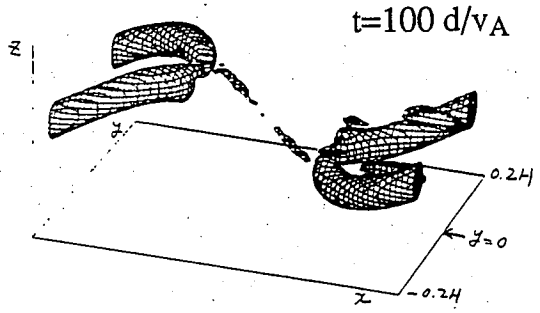

t=100 d/v_A

(d)

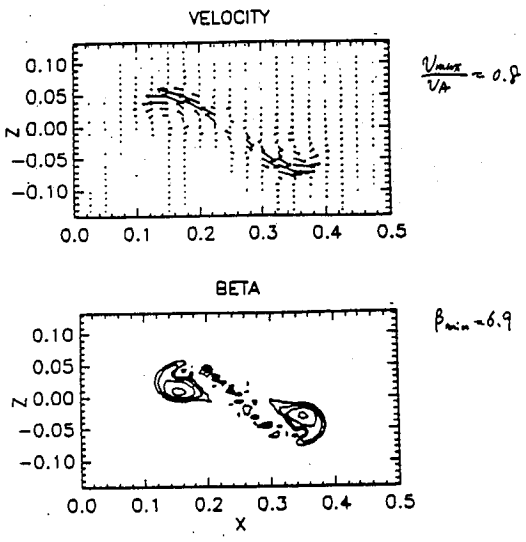

(e)

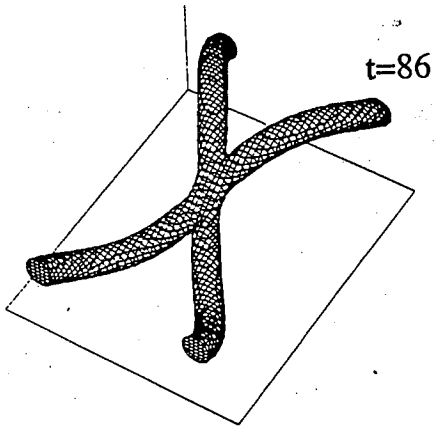

t=86 d/v_A

(f)

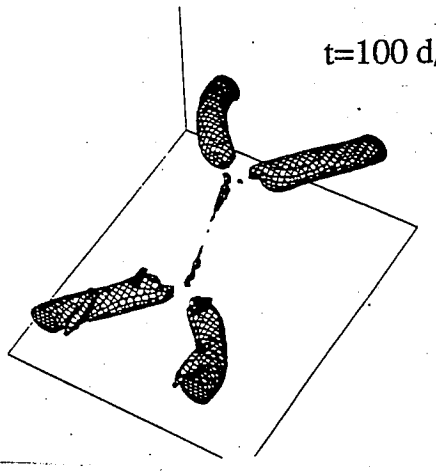

t=100 d/v_A

(g)

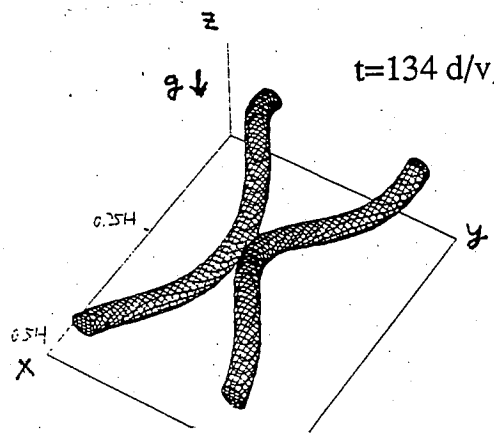

t=134 d/v_A

parallel helicity

(h)

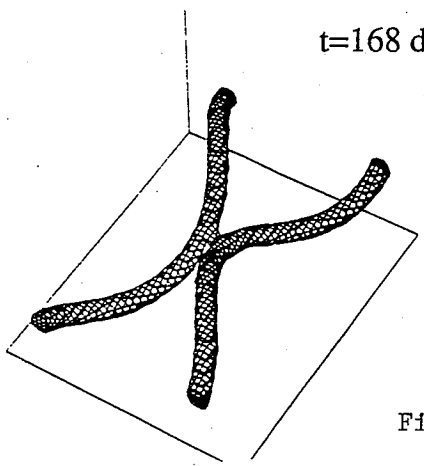

t=168 d/v_A

Fig. 4

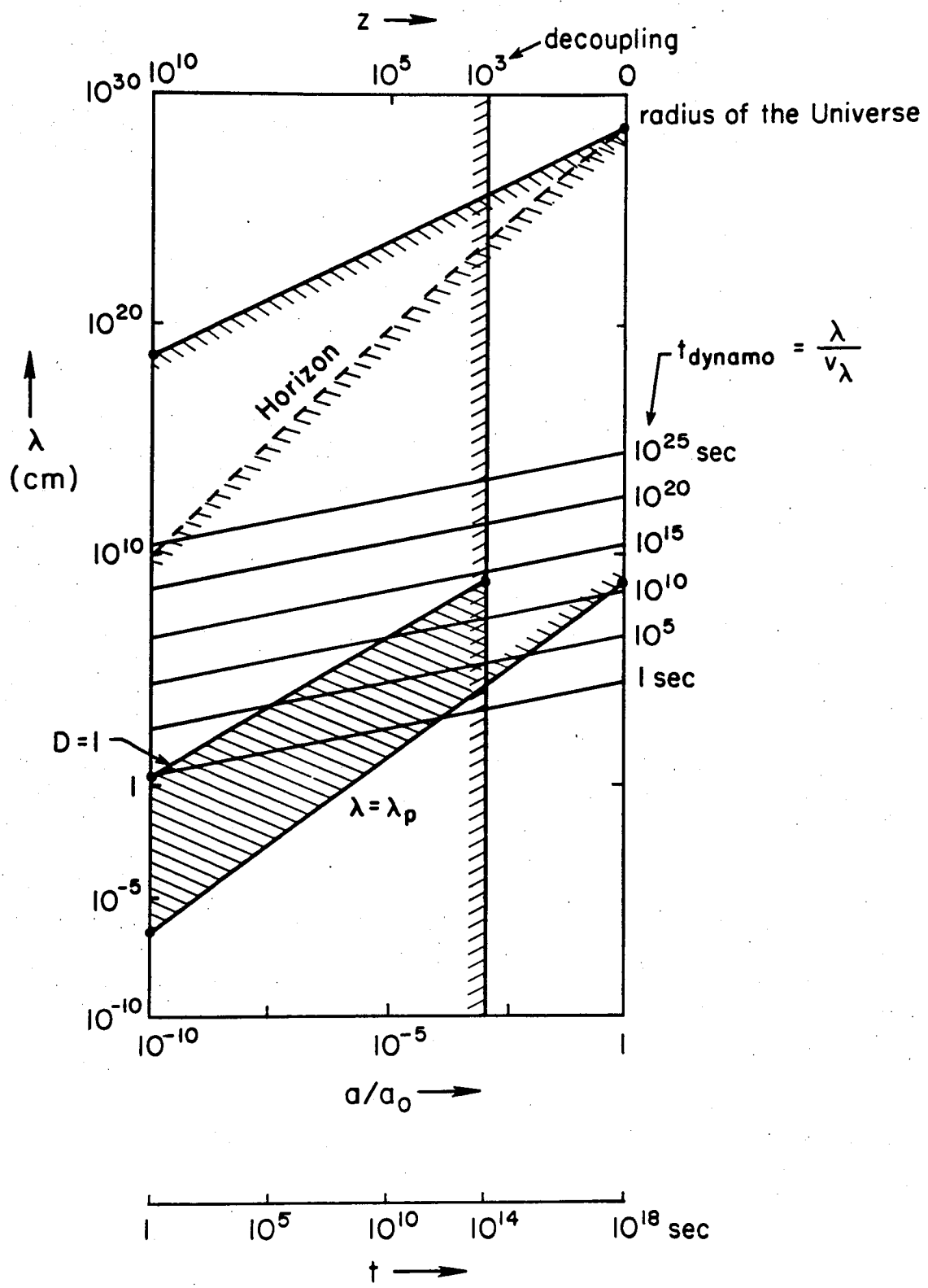
z
decoupling
10^{30} 10^{10} 10^{5} 10^{3} 0
radius of the Universe
10^{20}
Horizon
$t_{dynamo} = \frac{\lambda}{v_\lambda}$
λ (cm)
10^{25} sec
10^{20}
10^{15}
10^{10}
10^{5}
1 sec
10^{10}
D=1
1
$\lambda = \lambda_p$
10^{-5}
10^{-10}
10^{-10} 10^{-5} 1
a/a_0
1 10^{5} 10^{10} 10^{14} 10^{18} sec
t

Fig. 5

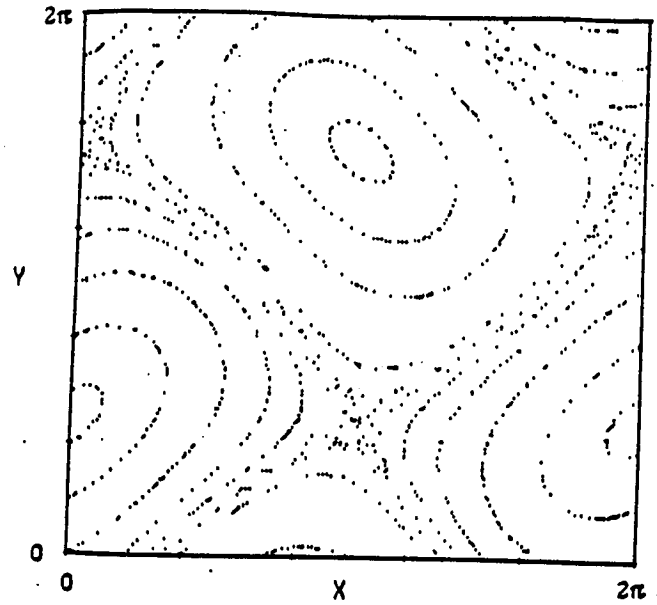

(a)

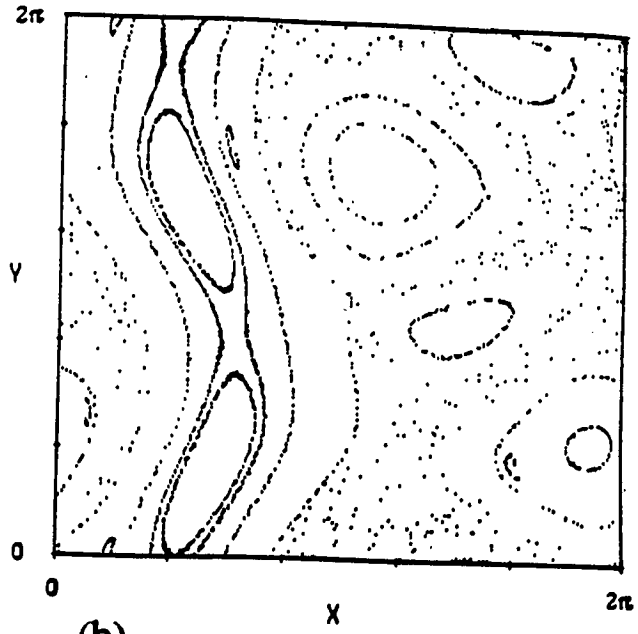

(b)

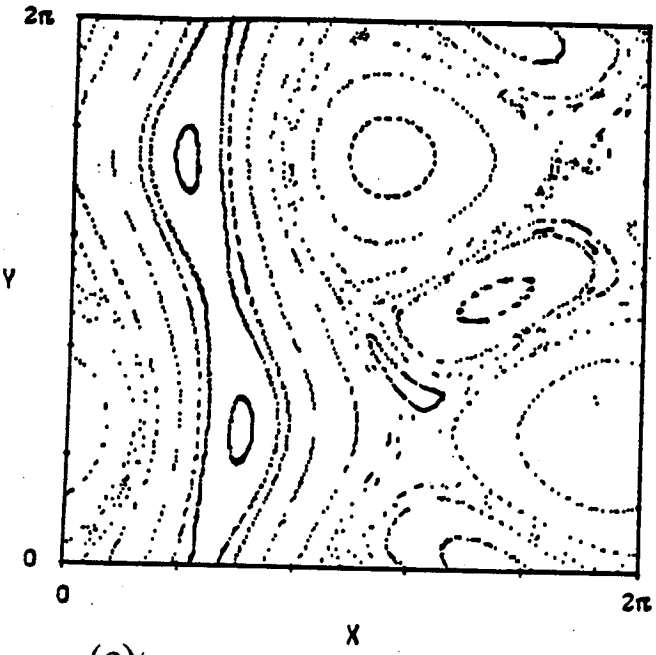

(c)

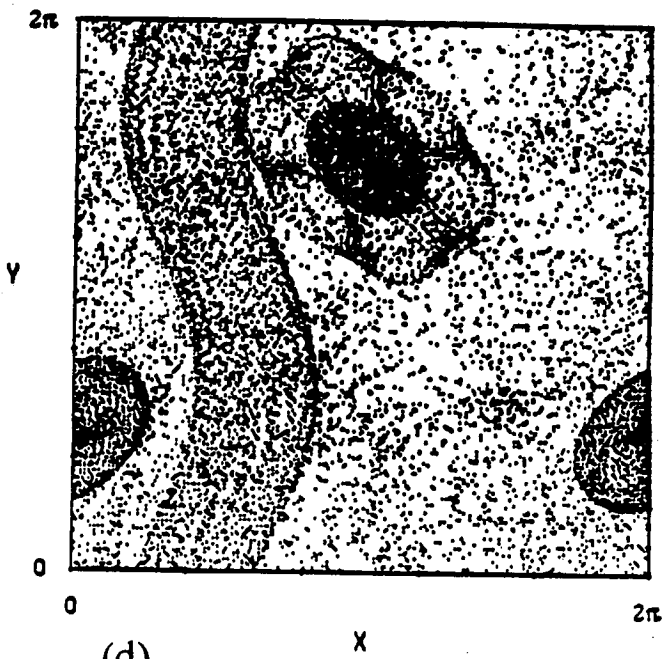

(d)

Fig. 6

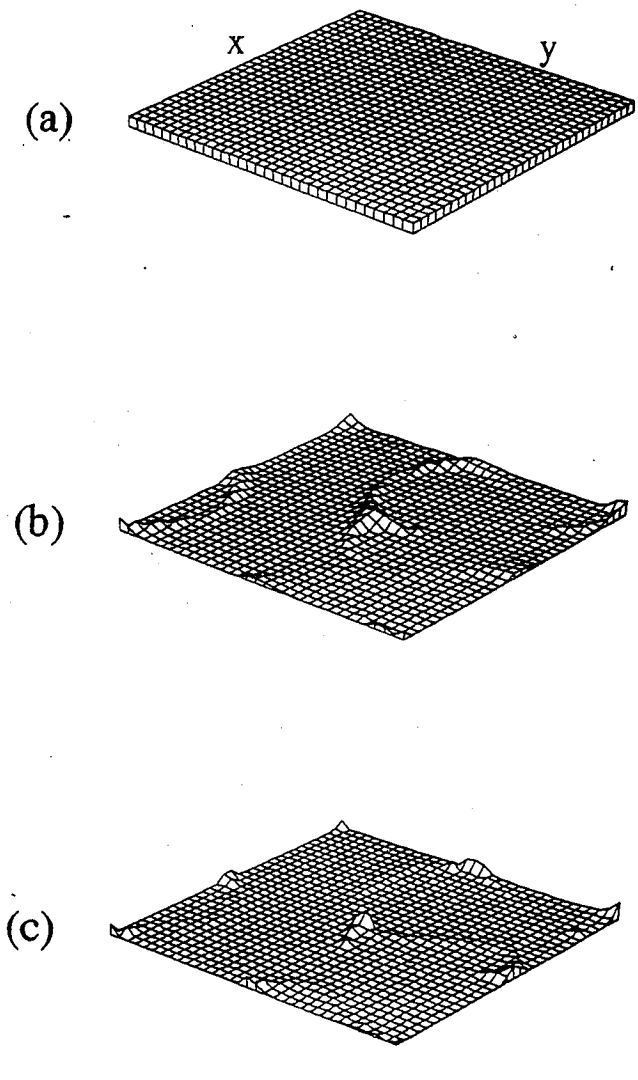

Fig. 7

(a)

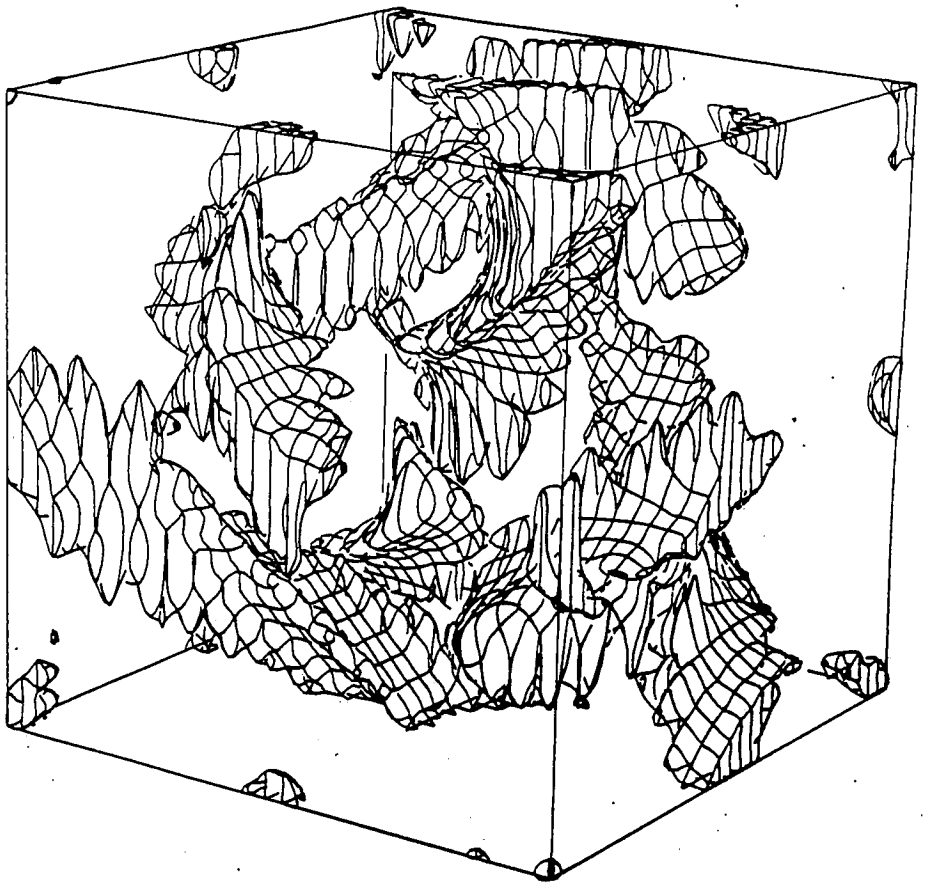

Fig. 8(a)

(b)

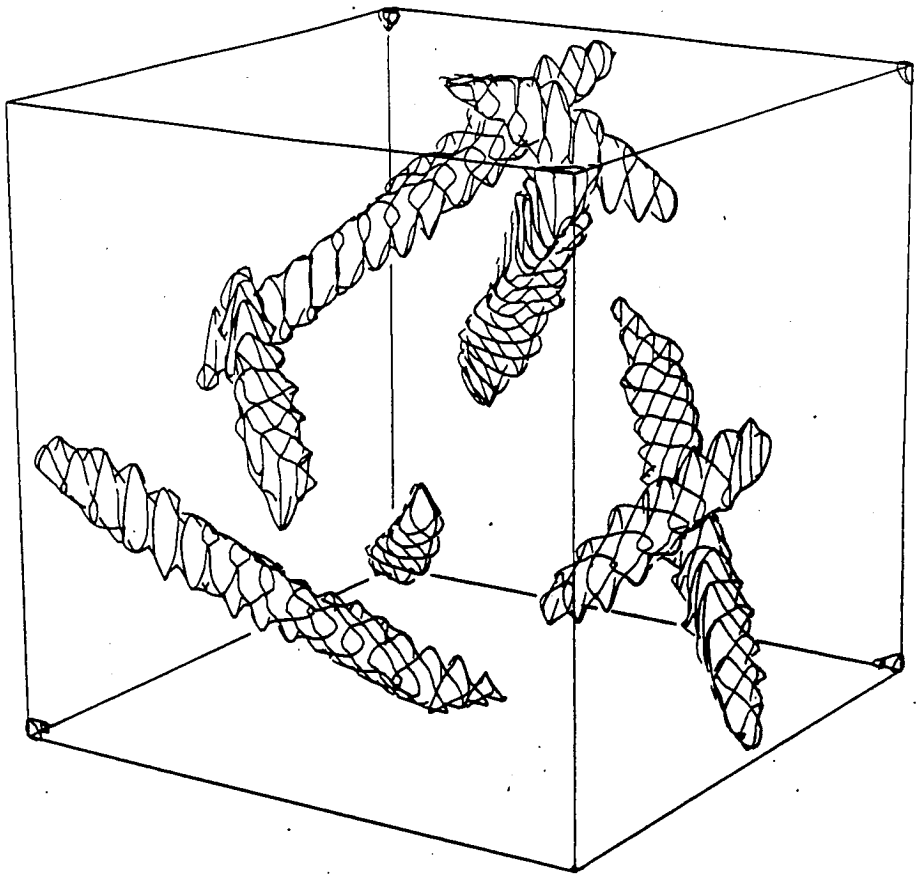

Fig. 8(b)

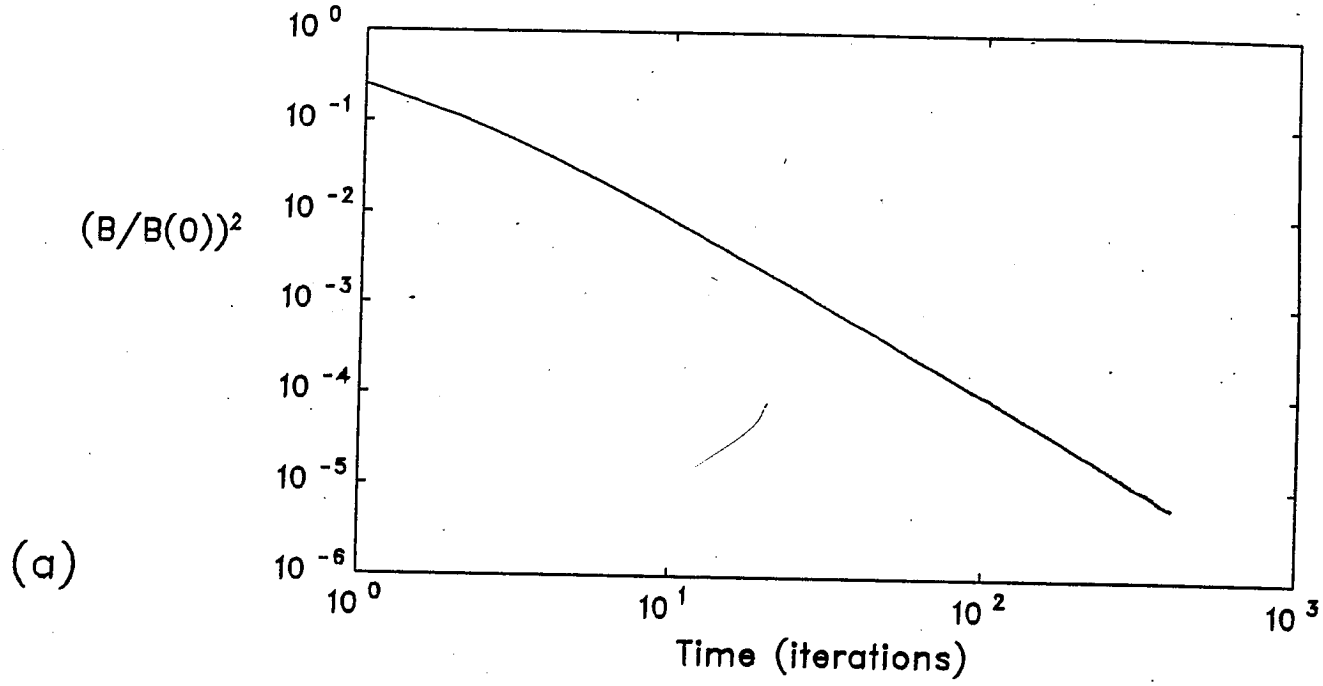
(a)
$(B/B(0))^2$
10^0
10^{-1}
10^{-2}
10^{-3}
10^{-4}
10^{-5}
10^{-6}
10^0
10^1
10^2
10^3
Time (iterations)

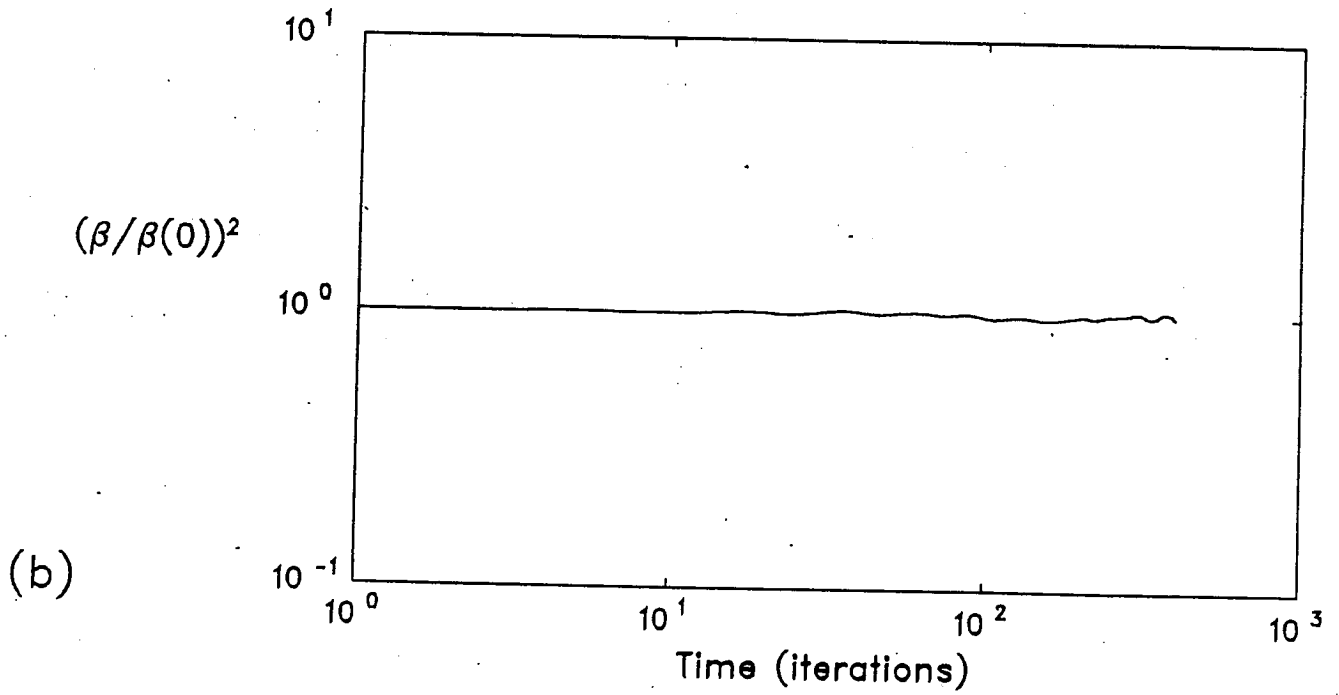
(b)
$(\beta/\beta(0))^2$
10^1
10^0
10^{-1}
10^0
10^1
10^2
10^3
Time (iterations)

Fig. 9

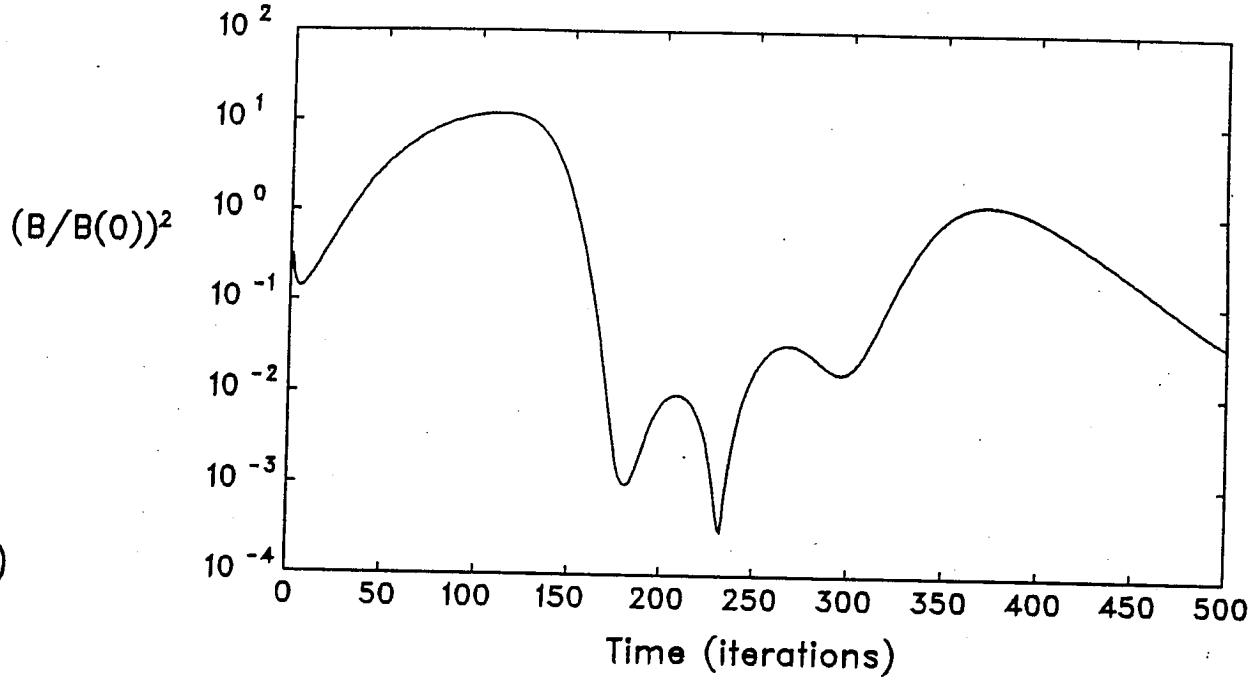
(B/B(0))²
10 2
10 1
10 0
10 -1
10 -2
10 -3
10 -4
0
50
100
150
200
250
300
350
400
450
500
Time (iterations)

(a)

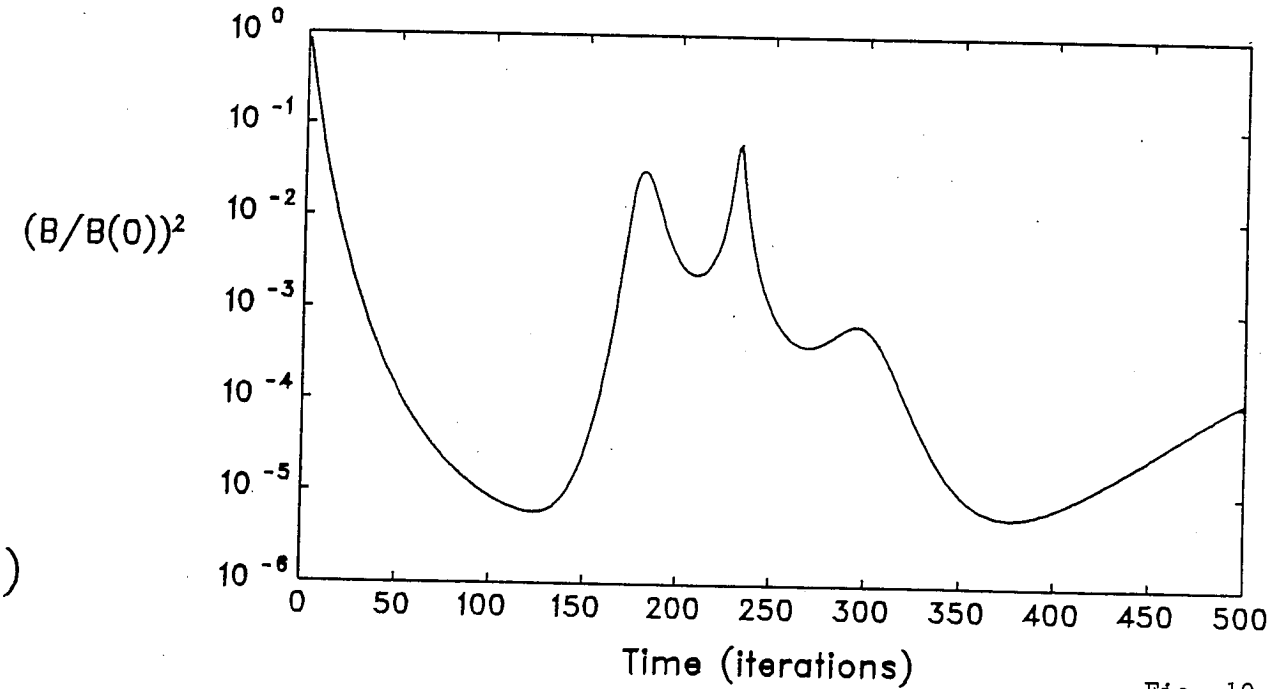
(B/B(0))²
10 0
10 -1
10 -2
10 -3
10 -4
10 -5
10 -6
0
50
100
150
200
250
300
350
400
450
500
Time (iterations)

(b)

Fig. 10

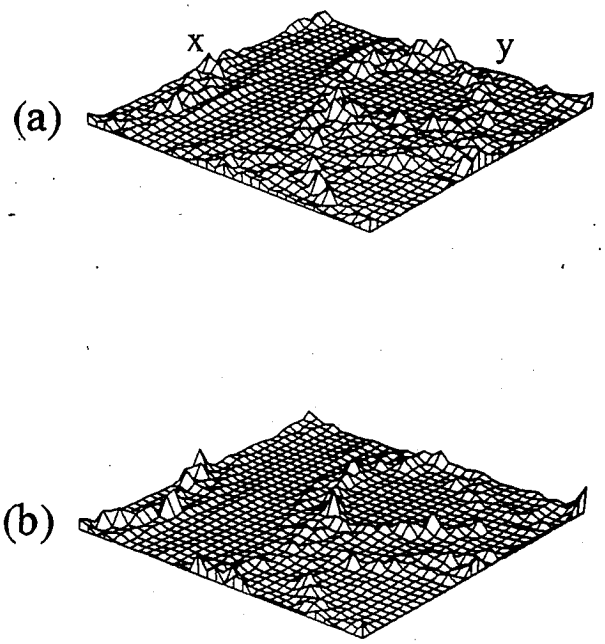

Fig. 11

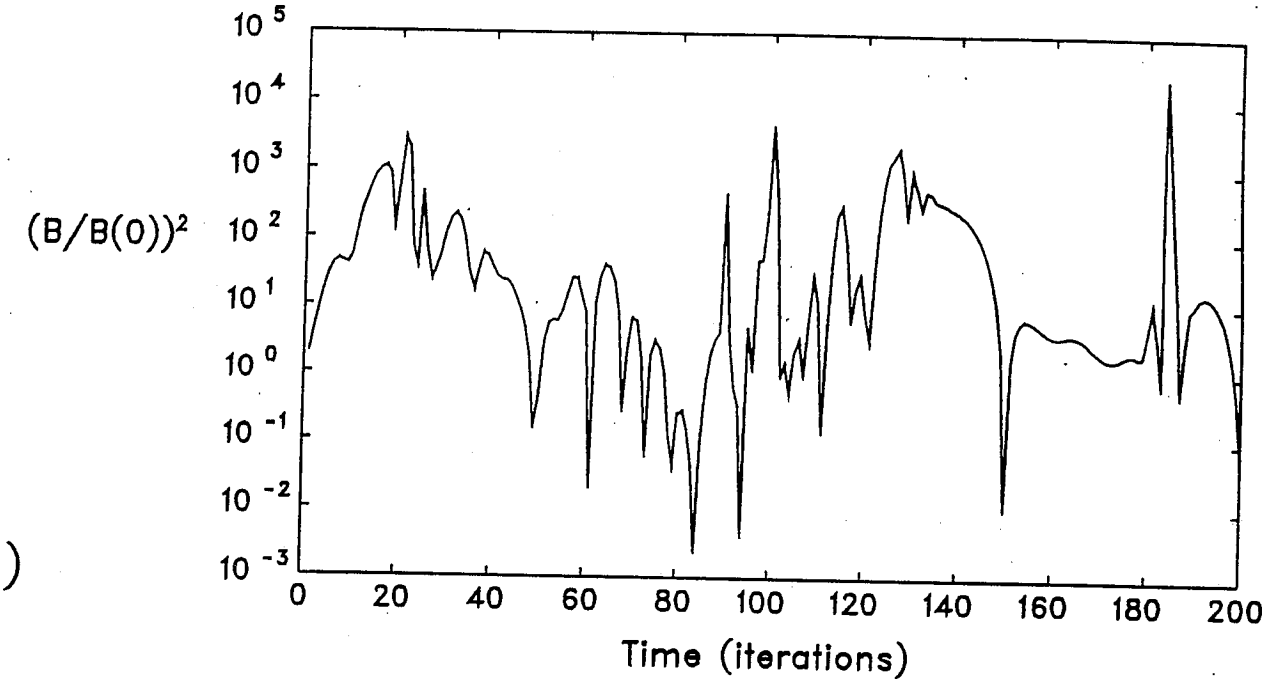
(B/B(0))²
10 5
10 4
10 3
10 2
10 1
10 0
10 -1
10 -2
10 -3
0
20
40
60
80
100
120
140
160
180
200
Time (iterations)

(a)

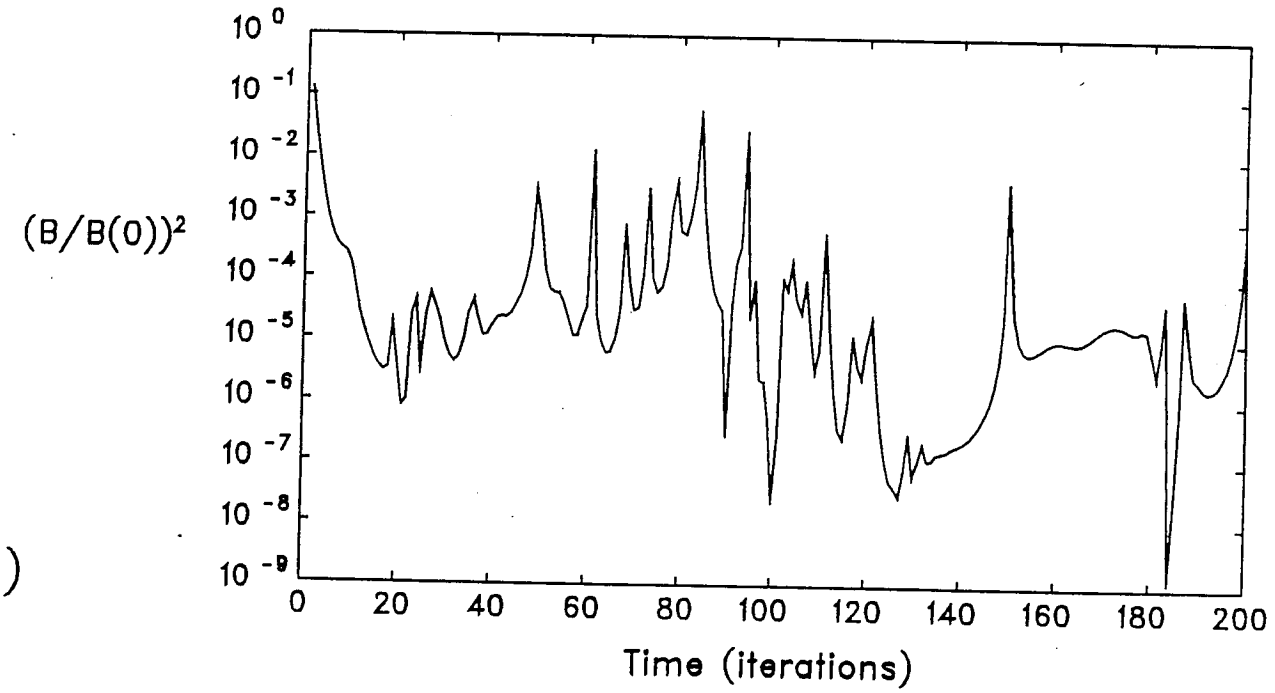
(B/B(0))²
10 0
10 -1
10 -2
10 -3
10 -4
10 -5
10 -6
10 -7
10 -8
10 -9
0
20
40
60
80
100
120
140
160
180
200
Time (iterations)

(b)

Fig. 12